Desalination and Water Treatment
www.deswater.com
doi: 10.1080/19443994.2014.996777

57 (2016) 4756–4768
March

Taylor & Francis
Taylor & Francis Group

Numerical investigation of the membrane fouling during microfiltration of semiconductor wastewater

Liu Jianxin, Liu Zhijun, Xu Xiaofei, Wei Wei, Wang Xiaojuan, Liu Fengxia*

Faculty of Chemical & Environmental & Biological Engineering, Dalian University of Technology, Dalian 116024, P.R. China, Tel. /Fax: +86 411 84986285; email: liufx@dlut.edu.cn (L. Fengxia)

Received 23 August 2014; Accepted 28 November 2014

ABSTRACT

Membrane fouling is a problem of vital importance in microfiltration. A numerical method was used to investigate the membrane fouling phenomenon during microfiltration of semiconductor wastewater. In the numerical model, the concentration-dependent physical properties were considered and a dynamically updating boundary condition was incorporated to deal with the flux variation with fouling resistance. The mechanism of suspension transition from liquid phase to gel phase was adopted to characterize the formation of membrane fouling. With this method, the flow field and the concentration distribution as well as the fouling resistance in the membrane module were obtained. The results revealed the mass transfer character in the concentration boundary layer and its influence on the formation of membrane fouling. The enhancement effect of cross-flow on membrane filtration was analyzed in terms of wall shear rate and dimensionless Peclet number. Agreement between the simulation and the experimental results demonstrated the applicability of this numerical method in evaluating membrane fouling during microfiltration.

Keywords: Cross-flow microfiltration; Fouling resistance; Computational fluid dynamics; Membrane fouling

1. Introduction

Compared with traditional physical and chemical separation processes, membrane filtration has shown such advantages as high water quality, little chemical addition, and low energy consumption. These processes can remove a wide range of contaminants such as suspended particles, organic matters, bacteria, and viruses et al. [1–4] and thus gain widespread applications in chemical, environmental, pharmaceutical, and biomedical engineering fields. The optimization design methods and corresponding researches of membrane filtration have allowed the selection of appropriate membranes for different processes [5–7]. Problems that limit the membrane filtration efficiency for pressure-driven membrane processes include a deterioration of the membrane fouling, an increase in the pressure, and a decrease in the flux, etc. [8–11].

Even though ingenious experiments have been designed and performed to investigate the concentration polarization and the corresponding fouling problems in membrane filtration, only qualitative or semi-quantitative results have been obtained, which are inadequate to gain a complete understanding of the fouling mechanism [12–15]. During the past decades, numerous theoretical researches have also been

*Corresponding author.

conducted to delve into this problem. One of the most classical theories is the stagnant film model proposed by Michaels [16]. Zydney [17] demonstrated the applicability of this model and extended it for the evaluation of the concentration polarization in filtration channels. By analogy with mass or heat transfer equations for a system with the same geometry as the membrane device, but with a non-permeable boundary, the mass transfer coefficient in the concentration polarization layer can be estimated based on the stagnant film theory [18]. Nevertheless, there are significant differences between permeable and impermeable systems [19]: (1) the local flow field in the feed channel is affected by the membrane permeability or resistance; (2) the solute concentration is non-uniform at the permeable boundary, but invariant at the impermeable boundary; (3) in permeable system, physical properties such as viscosity, density, and solute diffusivity near the membrane surface differ significantly from those in the bulk suspension. Therefore, the stagnant film model may lead to inaccuracies, especially for filtration with severe formation of fouling resistance.

Numerical mass transfer models for membrane filtration overcome the limitation of analytical or semi-analytical models since the number of simplifying assumptions regarding the velocity and the concentration fields is reduced [20–22]. Ghidossi et al. [9] reviewed the numerical techniques concerning the membrane processes and suggested that by prescribing appropriate boundary conditions for the flow and the concentration fields, the momentum and mass transfer governing equations could be solved by Finite Volume or Finite Element method. Rahimi et al. [23,24] used CFD simulations to investigate the local permeate and pressure distribution, as well as the influence of shear rate on membrane fouling in Microfiltration. Geralds et al. [20] performed finite volume simulations for the permeation of water through a nanofiltration membrane and validated their results with experiments. The authors emphasized the importance of taking into account the concentration-dependent physical properties, such as osmotic pressure, diffusivity of solute, and viscosity of suspension in numerical simulation. Aiming to provide methods for engineering design and analysis for membrane filtration process, Huang and Morrissey [25] used Finite Element method to simulate the development of the concentration polarization in the cross-flow ultrafiltration of Bovine serum albumin (BSA) suspensions. Their results showed that thin concentration boundary layer with steep gradient was developed in the vicinity of the membrane as the diffusion coefficient was quite small compared to the viscosity of the fluid in this region. Therefore, in order to capture the variation of the concentration normal to the membrane surface, sufficiently refined meshes must be formed near the membrane surface in the simulation. Richardson and Nassehi [26] pointed out that the main difficulty in modeling membrane filtration was the appropriate prescription of the concentration boundary condition at the porous walls, where the permeate flow and the wall concentration vary and interact with each other. Differing from the normal CFD simulation methods with fixed concentration or velocity boundary conditions, they developed an improved scheme where physical properties of the suspension at the permeate boundary dynamically changed. This method has been proved to be capable of taking into account the process dependency of physical and hydrodynamic parameters, as well as the coupling between velocity and concentration fields.

Previous numerical simulations for membrane processes mainly focused on RO or nanofiltration where the membranes have constant permeability or resistance. However, in ultrafiltration or microfiltration, the membrane fouling usually contributes to additional resistance to the permeate flow. In the wastewater treatment, membrane filtration is susceptible to fouling. Compared to the filtration of de-ionized water, the time required to attain the steady state filtration is longer and the trans-membrane pressure is higher for the filtration of wastewater under the same operation condition. Membrane fouling is more complicated because it is recognized as a group of physical and chemical effects [27]. Difficulties arise in simulation when taking into account the proper physical representation of fouling phase as well as the influence of fouling resistance on permeate flux decline. Numerous studies showed that membrane fouling was attributed to the accumulation of solutes or particles on the membrane, forming a layer termed as gel or cake layer [28,29]. In the research of membrane filtration of colloids, the transition of polarization concentration to consolidated cake was proposed by Chen et al. [30]. As the fouling forms, the suspension transits from the liquid-like phase with variable concentration to the solid-like gel phase with a constant concentration. For suspensions with particle size in the colloid range, which are usually treated in the Ultrafiltration and the Microfiltration process, Petsev et al. [31] and Jonnsson and Jonsson [32] suggested that the properties of concentrated suspensions can be related to osmotic pressure which in turn is influenced by the entropic effect and particle interactions. These authors pointed out that with an increase of concentration, the osmotic pressure theoretically passes a maximum which corresponds to the transition from the dispersive liquid-like

phase to the solid-like gel phase. In the case of membrane filtration, this transition can be used for the description of the fouling formation. Based on this theory, Bacchin et al. [33,34] established a unified model which is capable of predicting the concentration polarization and the fouling formation in the cross-flow Ultra-filtration. Schausberger et al. [35] applied CFD simulations to predict the concentration polarization and fouling during the Ultra-filtration of BSA solutions. Their numerical model incorporated the concentration-dependent physical properties as well as the phase transition theory. Agreement between the simulations and the experimental results demonstrates the applicability of the method in solving such membrane fouling problems.

In this study, a laboratory Microfiltration system was designed for the semiconductor wastewater purification. This study aimed for obtaining a better understanding of the fouling behavior on the membrane surface during filtration to facilitate design optimization. In the experiment, overall fouling resistances under several different operation conditions were tested. A specific CFD simulation model was developed to couple the hydrodynamic and mass transfer governing equations. Variations in physical properties such as viscosity, density, and generalized diffusivity with particle volume fraction were considered. Besides, the phase transition model was incorporated for the description of the fouling formation. Through the use of the numerical scheme with a dynamically updating boundary condition, the governing equations were solved for the flow and the concentration fields in membrane channels as well as the distribution of fouling resistance along the membrane surface.

2. Experiment setting

Properties of the membranes (ZF4120, Minglie, China) and the treated semiconductor wastewater are listed in Table 1. A Perspex filtration module with effective filtration area of 4,500 mm^2 (30 mm width by 150 m length) was used in all experiments. The feed channel had a cross-section of 60 mm^2 (30 mm width by 2 mm height). Flat sheet microfiltration membranes with a mean pore size of 0.25 μm was used in this study. The membrane was supported by the non-woven fabric and a perforated stainless steel plate to prevent distortion caused by trans-membrane pressure.

The membrane was soaked in de-ionized water for 2 h, then rinsed to wash away the impurity on membrane surface prior to use. In each run, the inherent membrane resistance R_m was tested by the dead-end filtration of de-ionized water under a trans-membrane pressure of 50 kPa and was confirmed to be $1.14 \pm 0.15 \times 10^{12}$ m^{-1}. The wastewater with a silica concentration of 1,800 mg/L which contains mainly silica after multiple pretreatments was got from a semiconductor manufacturer in south China and was chosen to be treated by the membrane filtration unit. Silica particle size distribution was measured by laser particle size analyzer (BT-9300, Better, China) and is shown in Fig. 1. The diameter was confirmed to be within the range of 0.1–2.0 μm with a mean value of 0.43 μm. This indicated that the majority of particles were greater in size than membrane pore diameter and could be sieved by the membrane.

A schematic diagram of cross-flow microfiltration system is shown in Fig. 2. This system could operate in both dead-end and cross-flow filtration modes. Valve I was kept open and valve II was closed when experiment was performed in the dead-end filtration mode. In the cross-flow filtration mode, magnetic pump was used to pump the feed suspension. Both valves were open and valve I was used to regulate the cross-flow rate. Pressure gauges on both feed and permeate sides were used to monitor the trans-membrane pressure. And the filtration was conducted in constant flux mode. At the permeate side of the membrane module, a peristaltic pump (DDBT-202, Zhixin, China) was applied to produce the trans-membrane pressure difference and pump the filtrate out at a constant permeate flow rate.

Fouling resistance was tested under several different conditions. During the experiment, the permeate flow rate was adjusted by changing the rotational speed of the peristaltic pump. Filtration continued until the pressure difference between the feed and permeation sides ΔP became steady. The feed flow

Table 1
Parameters of membrane properties and semiconductor wastewater

Feed suspension properties		Membrane properties	
Component	Silica	Material	PTFE
Mean particle diameter (μm)	0.43	Mean pore size (μm)	0.25
Particle density (kg/m^3)	2,390	Inherent resistance, R_m (m^{-1})	1.14×10^{12}
Feed concentration (mg/L)	1,800		

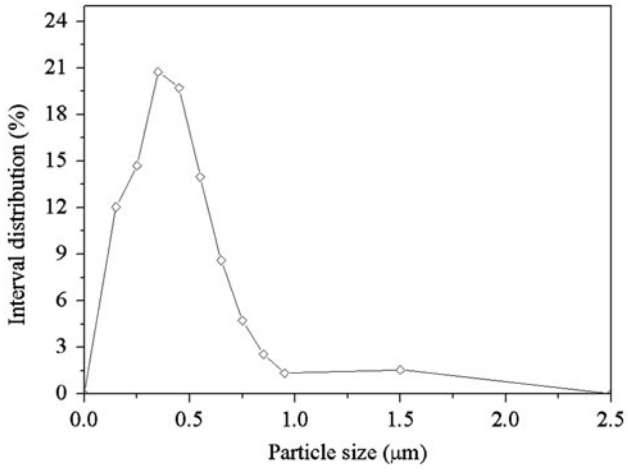

Fig. 1. Particle size distribution in semiconductor wastewater.

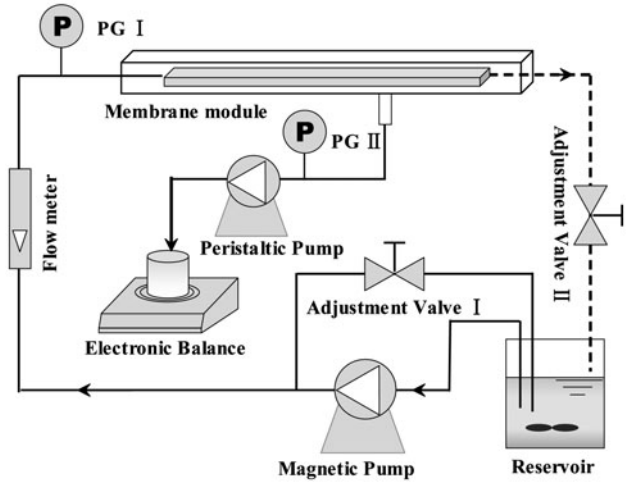

Fig. 2. Schematic of cross-flow microfiltration experiment flow chart.

was then switched instantaneously to de-ionized water. Experiment was terminated when the pressure difference arrived at a steady value again.

The fouling resistance was calculated by subtracting the inherent membrane resistance R_m from the overall resistance R_t using Darcy equation:

$$R_f = \frac{\Delta p}{\mu_l J} - R_m \tag{1}$$

where J is the average permeate flux through the membrane, R_f is the fouling resistance, ΔP is the trans-membrane pressure, and μ_l is the permeate viscosity.

3. Model developments

3.1. Mass transfer character near the membrane surface

As shown in Fig. 3, according to the characteristics of cross-flow filtration, the mass transfer layer above membrane surface can be classified into two regions: polarization layer with variable particle concentration and gel-layer with uniform concentration. In the polarization layer, particles flow along with the suspension and its concentration achieves a dynamically steady state. The particle concentration distribution in this layer can be obtained by solving the flow and mass transfer equations of quasi-liquid fluid. The particle concentration in the fouling gel-layer, however, should be determined from the phase transition from suspension to gel.

As suggested by Bacchin et al. [34], the osmotic pressure variation with respect to particle volume fraction can be used to determine the phase transition of colloid suspension. The osmotic pressure of suspension with interacting colloidal particles is considered as the superposition of the contributions from entropic, van der Waals interaction, and repulsive electrostatic interaction:

$$\Pi(\phi) = \Pi_{\text{entroy}}(\phi) + \Pi_{\text{vdw}}(\phi) + \Pi_{\text{elec}}(\phi) \tag{2}$$

where $\Pi_{\text{entropy}}(\phi)$ is the entropic osmotic pressure and can be approximated by Hall's hard sphere model as:

$$\Pi_{\text{entroy}}(\phi) = \frac{3k_BT}{4\pi a^3}\phi\frac{\left(1+\phi+\phi^2-0.67825\phi^3-\phi^4-0.5\phi^5-X\phi^6\right)}{1-3\phi+3\phi^2-1.04305\phi^3} \tag{3}$$

$\Pi_{\text{vdw}}(\phi)$ is the van der Waals osmotic pressure, k_B is the Boltzman constant, T is the temperature, and ϕ is

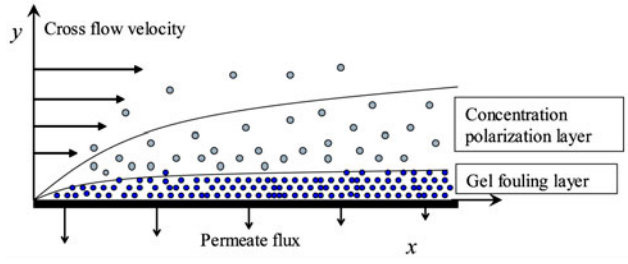

Fig. 3. Schematic drawing of colloidal particle concentration distribution on membrane surface.

the volume fraction of particles in the suspension. By differentiating the van der Waals free energy with respect to the number of neighboring particles, Jonsson and Jonsson [32] derived the following equation:

$$\Pi_{\mathrm{vdw}}(\phi) = \frac{H_A}{4\pi a^3}\frac{\phi^3}{\left(\phi_{\mathrm{cp}} - \phi_{\mathrm{cp}}^{1/3}\phi^{2/3}\right)^2} \tag{4}$$

where H_A is the Hamaker constant; a is the radius of the suspended particles.

$\Pi_{\mathrm{elec}}(\phi)$ is the osmotic pressure originating from electrostatic interactions. By solving the Poisson–Boltzmann equation and utilizing the Wigner-Seitz cell approach, Bowen and Jenner [36] obtained the following equation:

$$\Pi_{\mathrm{vdw}}(\phi) = \frac{(1-\phi)}{12}N_A k_B T c_0\left[\cosh\left(\frac{\kappa a e\zeta}{k_B T\left\{\kappa a\phi^{-1/3}\cosh[\kappa a(1-\phi^{-1/3})] + \sinh[\kappa a\left(1-\phi^{-1/3}\right)]\right\}}\right) - 1\right] \tag{5}$$

where c_0 is the ion concentration; κ is the inverse of Debye length; ζ is the zeta potential of colloid particles and N_A is the Avogadro's number.

Substituting the mean particle radius and other parameters into Eqs. (2)–(5), the osmotic pressure can be calculated and its variation with particle volume fraction is shown in Fig. 4. The values of osmotic pressure are extremely small compared to the trans-membrane pressure in microfiltration. Electrostatic interaction dominates the total osmotic pressure and increases with particle volume fraction to one maximum value and then decreases. Accordingly, the total osmotic pressure increases from zero to a maximum corresponding to the critical volume fraction ϕ_{crit}. Beyond this volume fraction, as Petsev et al. [31] pointed out, attractive interactions between particles would cause the suspensions to coagulate from the dilute (suspension) phase to aggregated (gel) phase which is consistent with the gel-layer fouling mechanism proposed by Michael [16]. In this paper, this critical volume fraction ϕ_{crit} was adopted to represent the transition from the concentration polarization phase to the fouling gel-layer phase. This transition is then incorporated into the numerical scheme to calculate the fouling resistance.

3.2. Governing equation

As shown in Fig. 3, feed suspension flows above the membrane surface in a tangential direction. Silica particles in suspension reach the steady state under both the convection and the diffusion mass transfer effects. The two-dimensional flow and mass transfer characteristics in membrane channel can be described by momentum and mass transfer equations for quasi-liquid.

The governing equations are listed in Table 2. Where u and v are the flow velocities along x and y direction, respectively; μ is the suspension viscosity; ρ is the suspension density. According to the volume fractions of flow fluid and silica particles, the mean density of suspension is calculated as:

$$\rho = \rho_l(1-\phi) + \rho_s\phi \tag{10}$$

For suspension with dispersed particles, viscosity variation with concentration should be considered. One

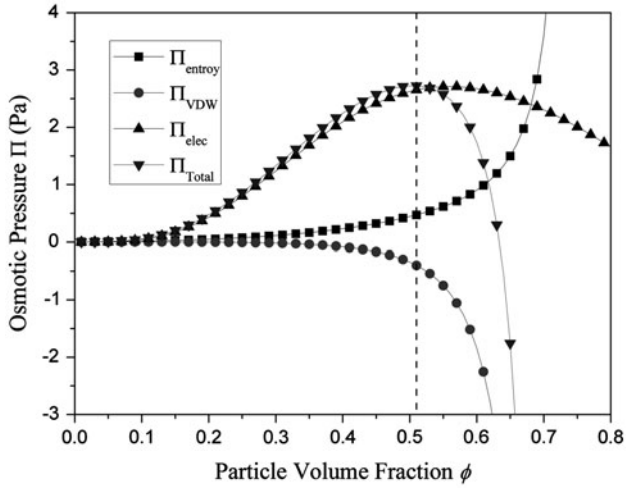

Fig. 4. Variation of osmotic pressure with particle volume fraction.

Table 2
Governing equations for the flow and mass transfer

Continuity equation	$\frac{\partial(\rho u)}{\partial x}+\frac{\partial(\rho v)}{\partial y}=0$ (6)
Navier–Stokes equations	$u\frac{\partial(\rho u)}{\partial x}+v\frac{\partial(\rho u)}{\partial y}=-\frac{\partial p}{\partial x}+\frac{\partial}{\partial x}\left(\mu\frac{\partial u}{\partial x}\right)+\frac{\partial}{\partial y}\left(\mu\frac{\partial u}{\partial y}\right)$ (7)
	$u\frac{\partial(\rho v)}{\partial x}+v\frac{\partial(\rho v)}{\partial y}=-\frac{\partial p}{\partial y}+\frac{\partial}{\partial x}\left(\mu\frac{\partial v}{\partial x}\right)+\frac{\partial}{\partial y}\left(\mu\frac{\partial v}{\partial y}\right)$ (8)
Mass transfer equation	$\frac{\partial(\rho u\phi)}{\partial x}+\frac{\partial(\rho v\phi)}{\partial y}=\frac{\partial}{\partial x}\left(\rho D\frac{\partial\phi}{\partial x}\right)+\frac{\partial}{\partial y}\left(\rho D\frac{\partial\phi}{\partial y}\right)$ (9)

commonly used correlation is the following equation introduced by Leighton and Acivos [37]:

$$\mu=\mu_l\left[1+1.5\frac{\phi}{1-\phi/0.58}\right]^2 \tag{11}$$

where μ_l is the viscosity of carrying fluid.

D is the generalized diffusion coefficient of the silica particles in suspension. For particles in the cross-flow channel, two kinds of diffusion mechanisms, shear-induced diffusion, and concentration gradient diffusion, work together to govern its mass transfer behavior. D is calculated by:

$$D=D_{SI}+D_g \tag{12}$$

where D_{SI} is the shear-induced diffusion coefficient, D_g is the concentration gradient diffusion coefficient.

Davis and Leighton [38] studied the particle migration behavior and derived the equation to calculate the shear-induced diffusion coefficient D_{SI}. For particles which have a mean radius of a and exist in the flow with a shear rate of γ, the shear induced diffusion coefficient D_{SI} is written as:

$$D_{SI}=1/13|\gamma|a^2\phi^2\left(1+0.5e^{8.8\phi}\right) \tag{13}$$

The concentration gradient diffusion coefficient, D_g, can be derived from the generalized Stokes–Einstein diffusivity equation which takes into consideration the derivative of osmotic pressure with respect to volume fraction and the particle sedimentation coefficient in the suspension K:

$$D_g(\phi)=D_\infty K(\phi)\frac{\phi}{nk_BT}\frac{d\Pi}{d\phi} \tag{14}$$

where $D_\infty=\frac{k_BT}{6\pi\mu a}$ is the generalized Stokes–Einstein diffusivity of the infinite dilution. For hard sphere, Happel cell model can be used to express the Sedimentation coefficient:

$$K(\phi)=\frac{6-9\phi^{1/3}+9\phi^{5/3}-6\phi^2}{6+4\phi^{5/3}} \tag{15}$$

3.3. Mesh and boundary condition

A two-dimensional simulation domain with a length of 150 mm and a height of 2 mm which was of the same size as the experiment module was formed (Fig. 5). Non-uniform construct grid was used to mesh the simulation domain with fine-grid treatment in the vicinity of the membrane boundary. Initially, a series of simulations were carried out to establish the adequately fine mesh for generating the grid-independent numerical solutions. The global convergence was evaluated in terms of the average fouling resistance, defined as:

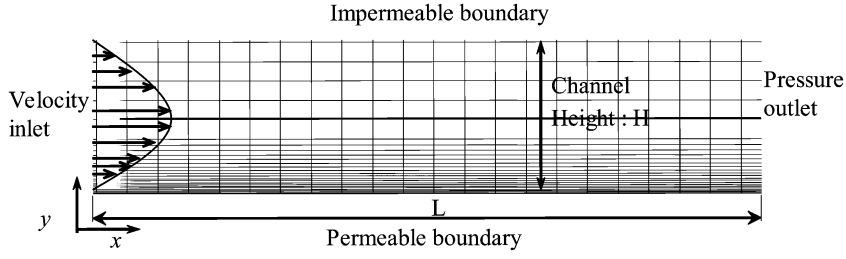

Fig. 5. Boundary condition and mesh in simulation.

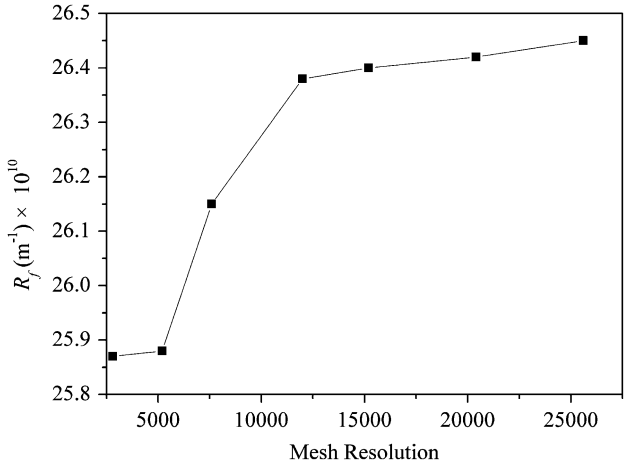

Fig. 6. Illustration of grid-independence of the numerical solution at the cross-flow velocity of 0.2 m/s (the mesh resolution is the total grid element in the solution domain).

$$\overline{R_f} = \int_0^l R_f dx \tag{16}$$

where R_f is the local fouling resistance along the membrane surface.

As shown in Fig. 6, $\overline{R_f}$became grid independent as the number of grid elements reached about 15,200. Therefore, this meshing scheme was adopted for all simulations.

Boundary conditions for flow and mass transfer are listed in Table 3.

Fully developed flow velocity profile was set at the entrance of the feed flow. In this study, the actual velocity distribution at this boundary was tested and verified with Particle Image Velocimetry. Particle volume fraction was given as feed suspension at the entrance. Where u_0 is the average cross-flow velocity; ϕ_0 is the particle volume fraction of the feed suspension. Top of the membrane channel was set with a non-slip impermeable wall boundary. As there is no particle permeating through this boundary, the particle flow flux and the gradient of volume fraction is zero. Suspension exits the channel from a free boundary where all changes of the parameters in the normal direction are equal to null.

As mentioned above, one of the most important features of microfiltration is that particles accumulate at the permeable membrane boundary and contribute to additional resistance to the permeate flow. Special considerations should be taken to deal with this boundary condition.

Firstly, the mass transfer conservation of particle volume fraction across this boundary is defined as:

$$\vec{V}\phi \cdot \vec{n} = -D\nabla\phi \cdot \vec{n} \tag{25}$$

where $\vec{V}$ is the velocity vector, $\vec{n}$ is the outward normal vector of the boundary face. This type of Robin boundary condition is given in an implicit form which cannot be directly incorporated into the discretized equations of the system. With the assumption of non-slip boundary condition for cross-flow velocity and complete rejection of the particles on the membrane surface, only the permeate flow contributes to the variation of the particle flux. Therefore, left side of Eq. (25) can be simplified as:

$$\vec{V}\phi \cdot \vec{n}\big|_{y=0} = -J\phi_w \tag{26}$$

The right side of Eq. (25) can be written in discretized form as:

$$D\nabla\phi \cdot \vec{n}|_{y=0} = D\frac{\phi_{w-}\phi_i}{dy} \tag{27}$$

Table 3
Flow and mass transfer boundaries

Boundary	Flow boundary condition	Mass transfer boundary condition
Inlet: $x = 0$ and $0 < y < H$	$u = 6u_0(yH - y^2)/H^2$ (17)	$\phi = \phi_0$ (21)
Top: $0 < x < L$ and $y = H$	$u = 0$, $v = 0$ (18)	$\frac{\partial\phi}{\partial y} = 0$ (22)
Exit: $0 < y < H$	$\frac{\partial u}{\partial x} = \frac{\partial v}{\partial x} = 0$ (19)	$\frac{\partial\phi}{\partial x} = 0$ (23)
Membrane: $0 < x < L$ and $y = 0$	$V_{wi} = \frac{\Delta P - \Pi(\phi_w)}{\mu(R_m + R_fi)}$ (20)	$\vec{V}\phi \cdot \vec{n} = -D\nabla\phi \cdot \vec{n}$ (24)

where ϕ_i is the volume fraction in the cell center adjacent to the permeate boundary, dy is the distance between this cell center and the boundary face center. Combining Eqs. (26) and (27), Eq. (25) can be replaced with:

$$J\phi_w = J\frac{D\phi_i}{D - Jdy} \tag{28}$$

This is a type of explicit boundary condition and can be treated directly with numerical methods.

Other aspects necessary to be considered include the fouling resistance to the permeate flow. This resistance is unknown prior to simulation, which makes the fixed velocity boundary condition unavailable. Based on the analysis in Section 3.1, the formation of fouling gel-layer can be determined from the critical particle volume fraction ϕ_{crit} of the phase transition. It is clear that the fouling resistance and the particle volume fraction interact with each other. In this work, a special numerical procedure with dynamically updating permeate boundary condition was applied to account for this interaction.

According to the generalized Darcy equation, the local permeate velocity V_{wi} along the membrane surface can be written as:

$$V_{wi} = \frac{\Delta P - \Pi(\phi_w)}{\mu(R_m + R_{fi})} \tag{29}$$

where ΔP is the trans-membrane pressure; R_{fi} is the local fouling gel-layer resistance; $\Pi(\phi_w)$ is the osmotic pressure of the suspension near the membrane surface. In the case of constant flux filtration, permeate flux can be drawn from the membrane module with average flow rate J which is expressed as:

$$J = \frac{1}{L}\int_0^L V_{\text{wi}}dx \tag{30}$$

During the simulation process, when the particle volume fraction ϕ_w is lower than the critical value ϕ_{crit}, only concentration polarization layer occurs in this mass transfer layer. A Volume fraction greater than ϕ_{crit} indicates the formation of the fouling gel-layer, then the local fouling resistance and the trans-membrane pressure should be increased in the next iteration step. The criteria for the increments of these two parameters is to maintain the average permeate flow rate calculated with Eq. (30) constant.

3.4. Solution scheme

The governing equations were discretized with Finite Volume Method and solved with an iterative scheme. For the solution of the momentum equation, SIMPLE algorithm was used to provide correction for the pressure and velocity field to satisfy the continuity condition.

During each iteration step of the numerical procedure, the viscosity and density of the suspension as well as the diffusion coefficient of the particles were updated based on the particle volume fraction obtained from the previous iterative step. The gel-layer resistance was calculated based on the principles presented in Sections 3.1 and 3.3 after the mass transfer equation was solved. In the next iteration step, the permeable boundary condition for the governing equations should be dynamically updated according to the local fouling gel-layer resistance.

4. Results and discussion

For the microfiltration of semiconductor wastewater in this study, three cross-flow velocities, 0.05, 0.1, and 0.2 m/s and a constant permeate flow rate of 3.0×10^{-6} m/s were applied to predict the fouling resistance and its distribution in the membrane channel. The results were compared with the corresponding experimental results.

4.1. Simulation results

Fig. 7 shows the variation of the local permeate velocity along the membrane surface. The permeate velocity tends to decrease from the entrance to the exit

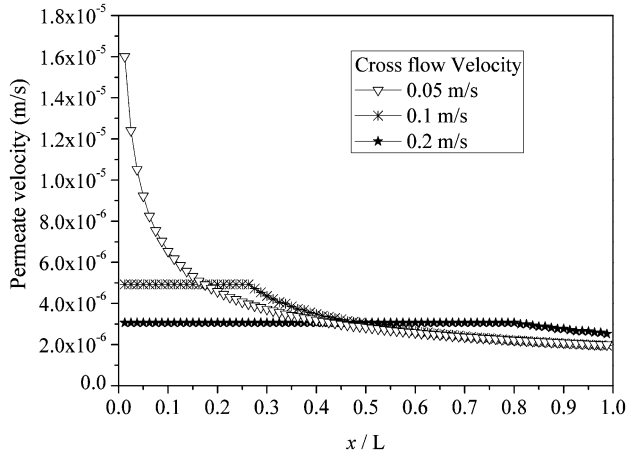

Fig. 7. Local permeate velocity variation along membrane surface.

of the membrane channel, which indicates an increase of the membrane resistance. Besides, constant permeate velocities near the entrance were observed under the cross-flow velocity of 0.1 and 0.2 m/s. According to the corresponding trans-membrane pressure results listed in Table 4, these constant velocities were extremely close to the permeate flux of pure water which means the intrinsic membrane resistance dominates in these regions.

Variation of the fouling gel-layer resistance along the cross-flow direction is shown in Fig. 8. As can be seen, the fouling resistance increases along the membrane surface and reaches the maximum values at the exit of the flow channel. With a decrease of the cross-flow velocity, the fouling layer gradually forms from the outlet to the inlet of the membrane channel. The membrane area covered with the fouling layer decreases with an increase in the cross-flow velocity. Under the cross-flow velocity of 0.2 m/s, the fouling layer constitutes 20.1% of the whole membrane surface, while as the cross-flow velocity changes from 0.1 to 0.05 m/s, the corresponding coverage ratio increases from 73.8 to 99.5%. Besides, the fouling resistance forming at the same position increases with a decrease in the cross-flow velocity.

In Fig. 9, the concentration polarization module (CP module, ϕ_w/ϕ_b) along the cross-flow direction is shown. The CP module increases from 1 at the entrance to a significantly great value at the exit. This is highly different from the cases of RO and nanofiltration where the permeate wall concentration is just several times larger than the bulk concentration. Theoretically, RO and nanofiltration mainly treats salt solution in which case, a small increase of concentration will result in a considerable increase of the osmotic pressure. This osmotic pressure is usually comparable with the trans-membrane pressure but poses opposite effect owing to the convective mass transfer, so the wall concentration for RO and nanofiltration can be maintained at a relatively low level. However, in the case of microfiltration, osmotic pressure of the concentrated suspension is extremely low, as shown in Fig. 4. Therefore, the increase of concentration on the membrane surface due to the convective mass transfer is more severe. Under these three conditions, all the CP modules develop to a constant value along the

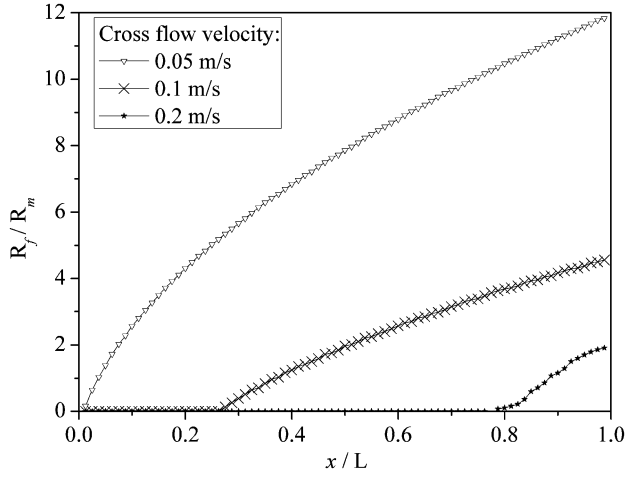

Fig. 8. Gel-layer resistance distribution along membrane surface.

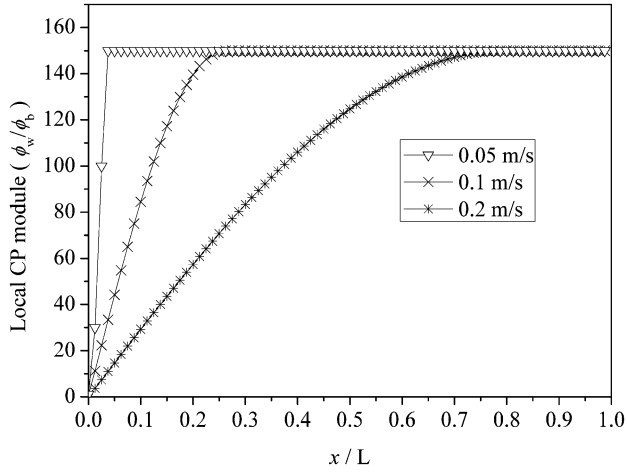

Fig. 9. CP modules distribution along membrane surface.

Table 4
Comparison between simulation and experimental results

Cross-flow velocity (m/s)		0.2	0.1	0.05
Trans-membrane pressure (Pa)	Simulation	4,210.5	10,569.9	3,0211.0
	Experiment	4,550	11,500	31,000
	Relative error	7.5%	8.1%	2.6%
Fouling resistance (10^{10} m^{-1})	Simulation	26.4	238.3	893.0
	Experiment	37.7	269.3	919.3
	Relative error	29.9%	11.5%	2.9%

membrane surface. Based on the phase transition principle, this constant CP module indicates the critical phase-transition concentration ϕ_{crit}. According to this critical concentration, the mass transfer boundary layer along the cross-flow direction can be divided into two parts: the developing boundary layer, and the double layers consisting of a developed boundary layer (with a maximum concentration of ϕ_{crit}) and a second fouling gel-layer which contributes to the fouling resistance. It is the full development of mass transfer boundary layer with double layers that affects membrane fouling.

The shear rate resulting from cross-flow velocity enhances mass transfer of microfiltration. The variation of shear rate in the vicinity of the membrane surface is shown in Fig. 10. It is observed that higher cross-flow velocity contributes to greater shear rate. With the boundary layer developing on the membrane surface, the overall flow rate decreases along the cross-flow direction. Therefore, a decline of shear rate is observed from the channel entrance to exit. According to Eqs. (12) and (14), the shear-induced diffusivity is two orders of magnitude higher than the concentration gradient diffusivity, especially in the concentrated suspensions. This demonstrates that the shear flow effect dominates the diffusion mechanism in the concentration polarization layer. As the shear-induced diffusion is proportional to shear rate, the particles in the fluid with a lower shear rate near the exit or under lower cross-flow velocities are more easily convected to the membrane surface, and, thus, result in more severe gel-layer fouling.

As is well known that the mass transfer near the membrane surface is governed by both convective and diffusive mechanisms, Peclet number is chosen to compare the relative influences of the two mechanisms. In the case of membrane filtration, Peclet number represents the ratio of convective transport V_w to diffusive transport D/δ in the concentration boundary layer, i.e.

$$Pe(x) = \frac{V_w(x)\delta(x)}{D_b} \tag{31}$$

where $V_w(x)$ is the local permeate flow velocity; D_b is the generalized diffusivity coefficient of the bulk suspension; $\delta(x)$ is the local thickness of the concentration boundary layer. Based on the mass transfer equilibrium, thickness of the layer can be calculated as:

$$\delta(x) = \frac{1}{V_w}\int_{\phi_b}^{\phi_w} \frac{D(\phi)}{\phi} d\phi \tag{32}$$

Fig. 11 shows that the Peclet number increases exponentially in the developing concentration boundary layer, while sharply reaches three constants, then remains constant at three different values as the fouling gel-layer forms. Even though the wall concentrations have the same value in the developed boundary layer as shown in Fig. 9, the mass transfer behaviors are different at the three cross-flow velocities. Bacchin et al. [34] termed this constant as critical Peclet number for the phase transition of suspensions from liquid to solid. In constant trans-membrane pressure filtration mode, they pointed out that the critical Peclet number stays constant under the same cross-flow velocity condition. From the result of this paper, it can be seen that

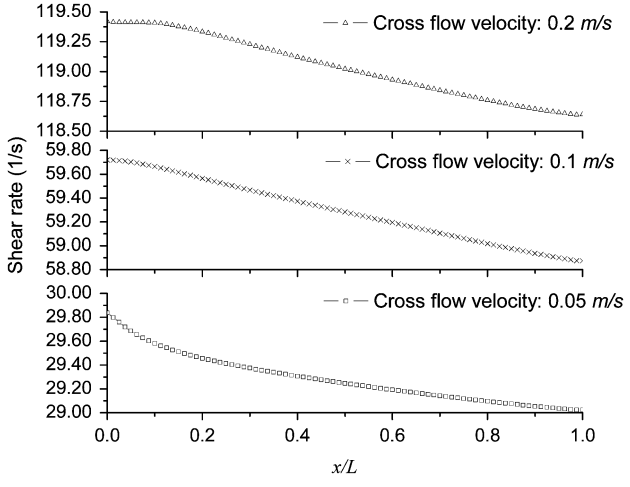

Fig. 10. Shear rate distribution in the vicinity of membrane along membrane surface.

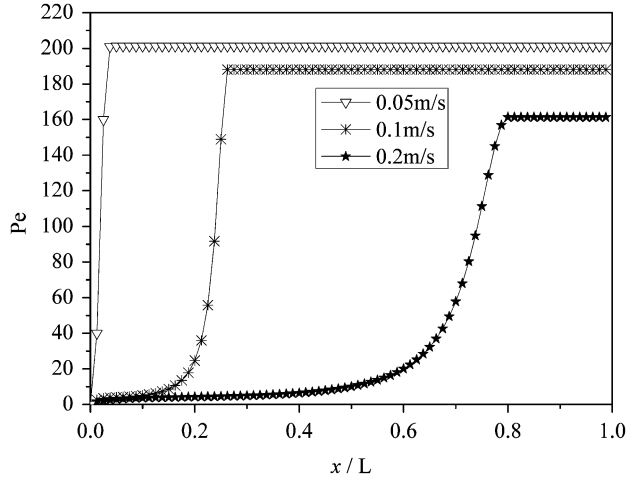

Fig. 11. Peclet number variation along membrane surface.

this value is also hydrodynamically dependent. Higher cross-flow velocity can decrease the Peclet number as well as postpone the Peclet number to reach its critical value on the membrane surface.

4.2 Experimental results

Table 4 shows the comparison between the simulation results and the experimental results. The results agree well with a maximum relative error of 8.1% for trans-membrane pressure. The fouling resistances obtained from the experiments are greater than the simulation values. This might be attributed to the size distribution of the silica particles in the suspension. In the microfiltration process, the majority of the particles are greater in size than the membrane pores and deposit on the membrane surface causing gel-layer fouling. However, smaller particles are inevitable to block the membrane pores and result in additional resistance, which is not considered in the numerical model of this paper. Therefore, the simulation results of the resistance is relatively smaller. As the cross-flow velocity increases from 0.05 to 0.2 m/s, the mass transfer on the membrane surface is enhanced, which results in a lower gel-layer resistance. The ratio of the gel-layer fouling resistance to the whole fouling resistance becomes smaller, while accordingly, the ratio of the blocking resistance to the whole fouling resistance becomes higher. Therefore, the difference between the predicted resistance and the experimental resistance is larger at the cross-flow velocity of 0.2 m/s. It also should be noted that as the cross-flow velocity decreases, the relative error of fouling resistance tends to get smaller. This indicates that with the development of the fouling gel-layer, the resistance changes from a pore-blocking dominated resistance to gel-layer fouling dominated one. And the resistance caused by pore-blocking contributes to a smaller proportion of the total resistance. The results prove that this simulation method can be applied to predict the fouling behavior in microfiltration with a significant surface fouling resistance.

5. Conclusions

This study investigated the fouling formation and the distribution of semiconductor wastewater in the cross-flow microfiltration of semiconductor wastewater. A mathematical model integrating the momentum and mass transfer governing equation as well as the phase transition characteristics of fouling was established. Contrary to normal simulation schemes with a fixed boundary condition, a numerical scheme involving a dynamically updating boundary condition was developed to account for the variation of the fouling resistance during the iterative computation. The results obtained in this study are concluded as follows:

(1) The gel-layer fouling distribution along the cross-flow direction was obtained from simulations. It is shown that the fouling resistance increases toward the exit of the flow channel. Increasing cross-flow velocity can effectively decrease the fouling resistance as well as the coverage ratio of the fouling layer on the membrane surface.
(2) According to the critical concentration of the formation of the gel-layer fouling, the mass transfer boundary layer can be divided into two parts: one is the developing region with the single concentration polarization layer and the other is the developed region with the coexistence of a concentration polarization layer and a fouling gel-layer. The development of the concentration polarization along the membrane surface is the critical factor resulting in the formation of the membrane fouling.

    Shear rate is an important factor that influences the transfer character of particles. Fouling usually arises and is serious at places where the shear rate is low, e.g., the channel exit. In normal flat channels, the shear rate decreases along the membrane surface. Decreasing the channel height along the feed flow direction can compensate for the decrease of shear rate. Besides, turbulence or eddies generated by the turbulence promoter will diminish or break the boundary layer, and, thereby, enhance mixing of the fluid in the vicinity of the membranes. Therefore, the fouling is effectively controlled.
(3) Even though the blocking phenomenon in the membrane pores is not considered in this model, which constitutes only a limited proportion of the whole fouling resistance and exists only at the initial stage of filtration, the simulation agrees with the experimental results well. This method is applicable for the prediction of gel-layer dominant fouling in membrane filtration.

Acknowledgment

The financial support from the PhD Start-up Fund of Natural Science Foundation of Liaoning Province (No. 20121024) is greatly acknowledged.

List of symbols

A	—	membrane surface area, m^2
a	—	particle radius, m
D	—	diffusion coefficient, m^2/s
H	—	height of membrane channel, m
H_A	—	Hamaker constant, 10^{-20} J
J	—	mean permeate flux, m/s
K	—	Happel correction for sedimentation velocity
k_B	—	Boltzman constant, 1.3806×10^{-23} J/K
L	—	length of membrane channel, m
N_A	—	Avogadro's number
n	—	particle number concentration, $1/m^3$
$\vec{n}$	—	outward normal vector of the boundary face
ΔP	—	trans-membrane pressure, Pa
Pe	—	Peclet number
Q	—	permeate flow rate, m^3/s
R_f	—	fouling resistance, 1/m
R_m	—	intrinsic membrane resistance, 1/m
T	—	temperature, K
u	—	velocity parallel to membrane surface, m/s
$\vec{V}$	—	velocity vector
v	—	velocity perpendicular to membrane surface, m/s
x	—	direction parallel to membrane, m
y	—	direction perpendicular to membrane surface, m

Greek Letters

δ	—	concentration boundary thickness, m
ϕ	—	particle volume fraction
γ	—	shear rate, s^{-1}
κ	—	inverse of Debye length, m^{-1}
ρ	—	suspension density, kg/m^3

Subscripts

0	—	inlet
b	—	bulk
cp	—	close packed
crit	—	critical
f	—	fluid
g	—	gradient
i	—	interior cell value adjacent to permeable boundary
l	—	liquid
s	—	solid
SI	—	shear induced
w	—	wall

References

[1] A.A. Alturki, N. Tadkaew, J.A. McDonald, S.J. Khan, W.E. Price, L.D. Nghiem, Combining MBR and NF/RO membrane filtration for the removal of trace organics in indirect potable water reuse applications, J. Membr. Sci. 365 (2010) 206–215.

[2] S.S. Sablani, M.F.A. Goosen, R. Al-Belushi, M. Wilf, Concentration polarization in ultrafiltration and reverse osmosis: A critical review, Desalination 141 (2001) 269–289.

[3] A.L. Zydney, Membrane technology for purification of therapeutic proteins, Biotechnol. Bioeng. 103 (2009) 227–230.

[4] A. Cassano, C. Conidi, L. Giorno, E. Drioli, Fractionation of olive mill wastewaters by membrane separation techniques, J. Hazard. Mater. 248 (2013) 185–193.

[5] K.M. Sassi, I.M. Mujtaba, Optimal design and operation of reverse osmosis desalination process with membrane fouling, Chem. Eng. J. 171 (2011) 582–593.

[6] S. Giglia, G. Straeffer, Combined mechanism fouling model and method for optimization of series microfiltration performance, J. Membr. Sci. 417 (2012) 144–153.
[7] E. Alventosa-deLara, S. Barredo-Damas, M.I. Alcaina-Miranda, M.I. Iborra-Clar, Ultrafiltration technology with a ceramic membrane for reactive dye removal: Optimization of membrane performance, J. Hazard. Mater. 209 (2012) 492–500.
[8] G. Belfort, R.H. Davis, A.L. Zydney, The behavior of suspensions and macromolecular solutions in crossflow microfiltration, J. Membr. Sci. 96 (1994) 1–58.
[9] R. Ghidossi, D. Veyret, P. Moulin, Computational fluid dynamics applied to membranes: State of the art and opportunities, Chem. Eng. Process. 45 (2006) 437–454.
[10] S.J. Tang, Z.W. Wang, Z.C. Wu, Q. Zhou, Role of dissolved organic matters (DOM) in membrane fouling of membrane bioreactors for municipal wastewater treatment, J. Hazard. Mater. 178 (2010) 377–384.
[11] Y. Marselina, P. Le-Clech, R.M. Stuetz, V. Chen, Characterisation of membrane fouling deposition and removal by direct observation technique, J. Membr. Sci. 341 (2009) 163–171.
[12] J.C. Chen, Q. Li, M. Elimelech, In situ monitoring techniques for concentration polarization and fouling phenomena in membrane filtration, Adv. Colloid Interface Sci. 107 (2004) 83–108.
[13] L.H. Cheng, Y.C. Yang, J.H. Chen, Y.H. Lin, S.H. Wang, A new view of membrane fouling with 3D ultrasonic imaging techniques: Taking the canola oil with phospholipids for example, J. Membr. Sci. 372 (2011) 134–144.
[14] S. Yao, M. Costello, A.G. Fane, J.M. Pope, Non-invasive observation of flow profiles and polarisation layers in hollow fibre membrane filtration modules using NMR micro-imaging, J. Membr. Sci. 99 (1995) 207–216.
[15] J. Altmann, S. Ripperger, Particle deposition and layer formation at the crossflow microfiltration, J. Membr. Sci. 124 (1997) 119–128.
[16] A.S. Michaels, New separation techniques for CPI, Chem. Eng. Prog. 64 (1968) 31–43.
[17] A.L. Zydney, Stagnant film model for concentration polarization in membrane systems, J. Membr. Sci. 130 (1997) 275–281.
[18] R. Ranjan, S. DasGupta, S. De, Mass transfer coefficient with suction for laminar non-Newtonian flow in application to membrane separations, J. Food Eng. 64 (2004) 53–61.
[19] J.M. Miranda, J.B.L.M. Campos, An improved numerical scheme to study mass transfer over a separation membrane, J. Membr. Sci. 188 (2001) 49–59.
[20] V. Geraldes, V. Semiao, M.N. de Pinho, Flow and mass transfer modelling of nanofiltration, J. Membr. Sci. 191 (2001) 109–128.
[21] M.N. de Pinho, V. Semiao, V. Geraldes, Integrated modeling of transport processes in fluid/nanofiltration membrane systems, J. Membr. Sci. 206 (2002) 189–200.
[22] A. Subramani, S. Kim, E.M.V. Hoek, Pressure, flow, and concentration profiles in open and spacer-filled membrane channels, J. Membr. Sci. 277 (2006) 7–17.
[23] M. Rahimi, S.S. Madaeni, K. Abbasi, CFD modeling of permeate flux in cross-flow microfiltration membrane, J. Membr. Sci. 255 (2005) 23–31.
[24] M. Rahimi, S.S. Madaeni, M. Abolhasani, A.A. Alsairafi, CFD and experimental studies of fouling of a microfiltration membrane, Chem. Eng. Process. 48 (2009) 1405–1413.
[25] L.H. Huang, M.T. Morrissey, Finite element analysis as a tool for crossflow membrane filter simulation, J. Membr. Sci. 155 (1999) 19–30.
[26] C.J. Richardson, V. Nassehi, Finite element modelling of concentration profiles in flow domains with curved porous boundaries, Chem. Eng. Sci. 58 (2003) 2491–2503.
[27] S. Shirazi, C.J. Lin, D. Chen, Inorganic fouling of pressure-driven membrane processes—A critical review, Desalination 250 (2010) 236–248.
[28] P. Bacchin, A possible link between critical and limiting flux for colloidal systems: Consideration of critical deposit formation along a membrane, J. Membr. Sci. 228 (2004) 237–241.
[29] S.T. Kelly, W.S. Opong, A.L. Zydney, The influence of protein aggregates on the fouling of microfiltration membranes during stirred cell filtration, J. Membr. Sci. 80 (1993) 175–187.
[30] V. Chen, A.G. Fane, S. Madaeni, I.G. Wenten, Particle deposition during membrane filtration of colloids: Transition between concentration polarization and cake formation, J. Membr. Sci. 125 (1997) 109–122.
[31] D.N. Petsev, V.M. Starov, I.B. Ivanov, Concentrated dispersions of charged colloidal particles—Sedimentation, Ultrafiltration and Diffusion, Colloids Surf., A 81 (1993) 65–81.
[32] A.S. Jonsson, B. Jonsson, Ultrafiltration of colloidal dispersions—A theoretical model of the concentration polarization phenomena, J. Colloid Interface Sci. 180 (1996) 504–518.
[33] P. Bacchin, M. Meireles, P. Aimar, Modelling of filtration: From the polarised layer to deposit formation and compaction, Desalination 145 (2002) 139–146.
[34] P. Bacchin, D. Si-Hassen, V. Starov, M.J. Clifton, P. Aimar, A unifying model for concentration polarization, gel-layer formation and particle deposition in crossflow membrane filtration of colloidal suspensions, Chem. Eng. Sci. 57 (2002) 77–91.
[35] P. Schausberger, N. Norazman, H. Li, V. Chen, A. Friedl, Simulation of protein ultrafiltration using CFD: Comparison of concentration polarisation and fouling effects with filtration and protein adsorption experiments, J. Membr. Sci. 337 (2009) 1–8.
[36] W.R. Bowen, F. Jenner, Dynamic ultrafiltration model for charged colloidal dispersions: A Wigner–Seitz cell approach, Chem. Eng. Sci. 50 (1995) 1707–1736.
[37] D. Leighton, A. Acrivos, Measurement of shear-induced self-diffusion in concentrated suspensions of spheres, J. Fluid Mech. 177 (1984) 109–134.
[38] R.H. Davis, D.T. Leighton, Shear-induced transport of a particle layer along a porous wall, Chem. Eng. Sci. 42 (1987) 275–281.